Mechanical Systems and Signal Processing 124 (2019) 664–678

Contents lists available at ScienceDirect

Mechanical Systems and Signal Processing

journal homepage: www.elsevier.com/locate/ymssp

Lower band gaps of longitudinal wave in a one-dimensional periodic rod by exploiting geometrical nonlinearity

Kai Wang [a,b], Jiaxi Zhou [a,b,*], Daolin Xu [a,b], Huajiang Ouyang [c]

[a] State Key Laboratory of Advanced Design and Manufacturing for Vehicle Body, Hunan University, Changsha 410082, PR China
[b] College of Mechanical and Vehicle Engineering, Hunan University, Changsha 410082, PR China
[c] School of Engineering, University of Liverpool, Liverpool L69 3GH, UK

ARTICLE INFO

Article history:
Received 9 December 2018
Received in revised form 20 January 2019
Accepted 6 February 2019

Keywords:
High-static-low-dynamic stiffness
Geometrical nonlinearity
Very low frequency
Longitudinal wave band gap
Wave filtering

ABSTRACT

In this paper, a local resonant (LR) rod with high-static-low-dynamic-stiffness (HSLDS) resonators is proposed to create a very low-frequency band gap for longitudinal wave propagation along the rod. The HSLDS resonator is devised by employing geometrical nonlinearity, and attached onto a periodic rod composed of rigid frames and rubbers to construct a LR rod. To reveal the band gaps, the LR rod is modeled as a lumped mass-spring chain. The effects of damping and nonlinearity of the HSLDS resonator on the dispersion relation is studied analytically by the Harmonic Balance method. The analytical results indicate that the damping mainly affects the width and depth of the band gap, while the nonlinearity can influence the central frequency and width of the band gap. In addition, both multi-body dynamic analyses and numerical simulations are conducted to predict longitudinal wave propagation along the LR rod, and thus to validate the very low-frequency band gap. The results show that the periodic rod with HSLDS resonators can create a very low-frequency band gap for longitudinal waves propagating along the rod.

1. Introduction

Frequency band generated by periodic structures presents means for wave attenuation. Phononic crystal or sonic metamaterials are examples of such structures, and the frequency band called band gap or stop band. Generally, there are two mechanisms for opening a band gap, namely Bragg scattering (BS) [1] and local resonance (LR) [2]. However, the band structure and wave attenuating feature caused by these two mechanisms are visibly different from each other. Specifically, the center frequency of the BS band gap is related to the wave velocity and lattice constant of a periodic structure, but that of the LR band gap is only dependent on the resonant frequency. Thus, the LR band gap can be formed at a much lower frequency than the BS band gap, considering the practical dimension of a periodic structure.

There are numerous studies about LR band gaps, as reviewed by Hussein et al. [3], but the literature review in this section does not try to be exhaustive, and only gives a brief review on the contributions to lowering LR band gaps and the works related to nonlinearity.

In order to form LR band gaps at low frequencies, many attempts to construct novel resonators have been made, such as in the form of a mass-spring device [4–7], a continuum beam [8,9], an inertial amplification mechanism [10], piezoelectric patches [11,12], electroactive polymer layers [13], a cylindrical tungsten pillar [14] and a ball coated with a soft material [2].

* Corresponding author at: College of Mechanical and Vehicle Engineering, Hunan University, Changsha 410082, PR China.
E-mail address: jxizhou@hnu.edu.cn (J. Zhou).

https://doi.org/10.1016/j.ymssp.2019.02.008
0888-3270/

Especially, the simple mass-spring resonator was modified to broaden the band gap or to achieve multiple band gaps, such as lateral local resonators [15], a multi-stage resonators [16], a local resonator with multi-oscillator [6] and a force and moment resonator [17]. The results of these studies show that the local resonator can successfully create band gaps in low frequency range. However, because of the restrictive space and load-supporting capability of the resonator, it might be impossible to design a local resonator with ultra-large mass and ultra-low stiffness in a traditional way, and thus it is still a challenge for phononic control in the ultra-low frequency domain [3].

Fortunately, a high-static-low-dynamic stiffness (HSLDS) can be realized by exploiting geometrical nonlinearity [18–25]. In our previous works [26,27], a local resonator with HSLDS was proposed to create a band gap of bending wave in very low frequency region along an Euler-Bernoulli beam. The HSLDS property was obtained by using the negative-stiffness (NS) mechanism to neutralize the positive stiffness partially, so that the residual stiffness of the oscillator can be tuned towards zero. Therefore, the local resonator containing the NS mechanism is a promising solution for shifting the band gap from a high frequency region to a low one.

Nevertheless, the HSLDS has nonlinear attributes related to displacements and geometry. When the resonator undergoes large-amplitude oscillation, the effects of nonlinearity on the dispersions and band gaps cannot be ignored. In such a situation, the characteristics of nonlinear wave propagating along the sonic periodic structures should be investigated, which would provide valuable guidance for the application of nonlinear local resonators.

The dispersion features of a one-dimensional chain attached with nonlinear resonators have been studied widely. Lazarov and Jensen [28] revealed the band structure of a chain with local resonators possessing cubic nonlinearity. Fang et al. [29] attached oscillators with cubic stiffness to a chain to construct a nonlinear acoustic metamaterials and studied its dispersion feature. Chakraborty and Mallik [30] analyzed the wave propagation characteristics in a nonlinear periodic chain by using the perturbation approach. Manktelow et al. [31] studied the weakly nonlinear wave interactions in a periodic structure by using perturbation method of multiple time scales and proposed several potential applications of nonlinear wave interactions. Rothos and Vakakis [32] presented the dynamic interactions of travelling waves propagating in a linear chain with local essentially nonlinear attachments. Khajehtourian and Hussein [33] studied the band gap opened by a one-dimensional (1D) nonlinear elastic metamaterial with spring-mass resonators and analyzed the effect of nonlinearity on the band gap.

In this paper, a local resonator containing an NS mechanism with geometrical nonlinearity is proposed to filter low-frequency longitudinal waves in a one-dimensional periodic rod. Note that, the NS mechanism is employed to neutralize the stiffness of the positive-stiffness element, and thus to construct an HSLDS resonator in this paper, which is completely different from those works [21,34,35] where the NS mechanism is used to construct a bistable resonator with pure negative stiffness. The stiffness of the HSLDS resonator can be tuned to any desired low values by adjusting the NS mechanism provided that the resonator does not undergo large-amplitude oscillations. A lumped mass-spring model is established to reveal dispersion properties and demonstrate band structures theoretically by using the Harmonic Balance method, which are also validated by numerical simulations.

This paper is organized as follows. In Section 2, the static analysis is carried out to show the tunable-low-stiffness feature of the local resonator. Then, the band structure of a longitudinal wave propagating in the LR rod is obtained theoretically and numerically in Section 3. In Section 4, the effects of both the number of unit cells and excitation amplitude on the wave attenuation performance are studied. Finally, some conclusions are drawn in Section 5.

2. Stiffness feature of the HSLDS local resonator

The physical model of a one-dimension periodic rod with HSLDS local resonators is shown in Fig. 1. All the masses and springs of the HSLDS resonator are installed in the same horizontal plane. Therefore, the gravity of the mass is not considered in the static analysis, which is different from the HSLDS resonator in our previous work [27]. The resonator consists of a mass, two relaxed horizontal springs and two pre-compressed vertical springs. For each spring, one end is connected to the mass, while the other end is connected to a rigid frame. Two nearby frames are connected by a rubber block (black area in Fig. 1). When the mass deviates from the static equilibrium along the horizontal direction, the vertical springs become oblique and form a NS mechanism due to the geometrical nonlinearity. Hence, a tunable low stiffness can be realized by employing such a NS mechanism to counteract the positive stiffness of the horizontal springs.

When the resonator is at rest, the configuration of the resonator is shown in Fig. 2a. Note that the resonator mass can only move in the horizontal direction, and two vertical springs deform symmetrically with respect to the horizontal springs. When an external load f is applied on the mass along the horizontal direction, the resonator mass will deviate from the static

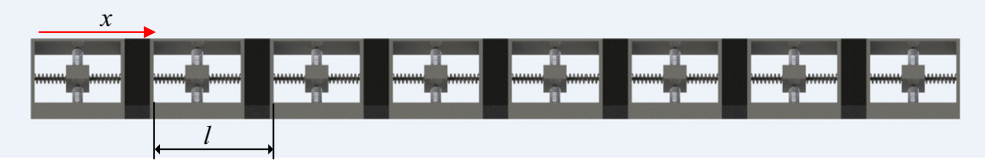

Fig. 1. The physical model of the HSLDS-LR one-dimensional periodic rod with lattice constant l.

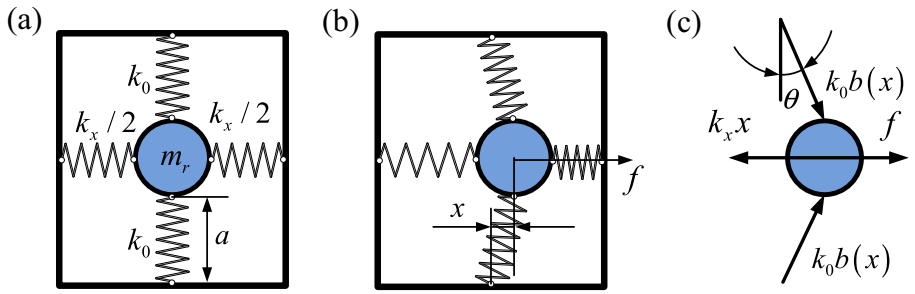

Fig. 2. Schematic diagram of static analysis of the HSLDS resonator (top view). (a) Rest configuration, (b) deformed configuration and (c) free-body diagram of the resonator.

equilibrium by a distance x, as depicted in Fig. 2b. In the deformed configuration, one of horizontal springs is compressed but the other is stretched, and deformations of these two springs are equal.

Note that a parameter η is introduced to denote the ratio of the net stiffness of the HSLDS resonator at the static equilibrium position after neutralization by the NS mechanism to the stiffness of the horizontal springs k_x [27]. By changing η from 1 to 0, the stiffness of the HSLDS resonator can be tuned towards a desired low value and even zero.

The free-body diagram of the mass is drawn in Fig. 2c. From the equilibrium of forces acting on the mass, one can obtain the relationship between the restoring force f and the displacement x. The procedure for deriving both the force and stiffness expressions of the HSLDS resonator is the same as that in our previous work [27]. For the sake of brevity, the restoring force f_{HSLDS} and the stiffness k_{HSLDS} of the HSLDS resonator are given directly by

$$f_{\mathrm{HSLDS}} = k_x x - (1-\eta)\frac{ax}{b_o - a}\left(\frac{b_o}{\sqrt{a^2 + x^2}} - 1\right) \tag{1}$$

$$k_{\mathrm{HSLDS}} = k_x - (1-\eta)\frac{a}{b_o - a}\left[\frac{a^2}{(a^2 + x^2)^{\frac{3}{2}}} - 1\right] \tag{2}$$

where k_x is the stiffness of the horizontal spring, a is the deformed length of the vertical spring at the static equilibrium position and b_o is the relaxed length of the vertical spring.

By dividing both sides of Eq. (1) by $k_x b_0$ and dividing both sides of Eq. (2) by k_x, respectively, the dimensionless restoring force $\bar{f}_{\mathrm{HSLDS}}$ and stiffness $\bar{k}_{\mathrm{HSLDS}}$ of the HSLDS resonator can be given by

$$\bar{f}_{\mathrm{HSLDS}} = \bar{x} - (1-\eta)\frac{\bar{a}}{1-\bar{a}}\left(\frac{1}{\sqrt{\bar{a}^2 + \bar{x}^2}} - 1\right)\bar{x} \tag{3}$$

$$\bar{k}_{\mathrm{HSLDS}} = 1 - (1-\eta)\frac{\bar{a}}{1-\bar{a}}\left[\frac{\bar{a}^2}{\left(\bar{a}^2 + \bar{x}^2\right)^{\frac{3}{2}}} - 1\right] \tag{4}$$

where $\bar{x} = x/b_0$ and $\bar{a} = a/b_0$.

It should be noted that the above restoring force and stiffness are achieved under the so-called *zero-stiffness* condition [27], which demonstrates a unique relationship between the stiffness ratio $\varepsilon = k_o/k_x$, the geometrical parameter $\bar{a} = a/b_0$, and the net stiffness ratioη, as given by

$$\varepsilon = \frac{(1-\eta)\,\bar{a}}{2\left(1-\bar{a}\right)} \tag{5}$$

From Eq.(5), one can see that the net stiffness ratio η can be tuned to be any targeted values from 0 to 1 by adjusting the stiffness ratio εor the geometrical parameter $\bar{a}$.

To sum up, the main procedure of designing the HSLDS resonator can be listed as follows. Firstly, for a target band gap frequency ω_t, the net stiffness ratio $\eta = (\omega_t/\omega_0)^2$ is determined, where ω_0 is the natural frequency of the resonator without the NS mechanism. Then, the parameters of the resonator are designed under the constraint described by Eq. (5).

From Eq. (4), it can be seen that the non-dimensional stiffness of the HSLDS resonator is equal to η only at the static equilibrium ($\bar{x} = 0$), and increases with the displacement increasing, which presents a feature of hardening-stiffness nonlinearity.

To broaden the displacement range where the stiffness is close to the targeted value η as much as possible, the optimal value of $\bar{a}_{opt} = (2/3)^{3/2}$ is selected [27].

For the HSLDS resonator, the non-dimensional stiffness against the displacement for different ratios of residual stiffness are shown in Fig. 3 when $\bar{a} = (2/3)^{3/2}$. As seen from Fig. 3, in the vicinity of the static equilibrium, the stiffness is close to the targeted value η. In the displacement range $\left(-\bar{x}_{\mathrm{dmax}},\ \bar{x}_{\mathrm{dmax}}\right)$, $\bar{x}_{\mathrm{dmax}} = 2\sqrt{3}/9$, as presented by a gray rectangular area, the non-dimensional stiffness is lower than 1, which implies that the dimensional stiffness is smaller than k_x.

3. Band gaps generated by HSLDS local resonators

3.1. Equations of motion

In order to analyze the band features of longitudinal waves, the HSLDS-LR periodic rod is modeled as a lumped mass-spring chain, as shown in Fig. 4a. The frame of the resonator is much stiffer than the rubber block, and thus only the stiffness of the rubber block is taken into account to calculate the equivalent stiffness of the connecting spring. The frame of the resonator is simplified as a mass and the rubber block is simplified as a spring with stiffness [36]

$$k = 3.6G\left[1 + 2.22\left(\frac{ab}{2(a+b)h}\right)^2\right]\frac{ab}{h} \tag{6}$$

where a, b, h and G are the length, width, height and shear modulus of the rubber block, respectively. The damping of the resonator is mainly caused by the friction between each connecting parts, which is hard to be determined theoretically. Thus, a linear viscous damper is employed to take into account the energy dissipation in the chain.

The parameters of the HSLDS-LR periodic rod are listed in Table 1. The length of the HSLDS-LR periodic structure is assumed to be infinite for the purpose of deriving the dispersion relation of this structure. $k_{\mathrm{HSLDS}}(x)$ denotes the nonlinear stiffness of the HSLDS-LR. In Fig. 4b, the region $[-\pi/l,\ \pi/l]$ represents the first Brillouin zone of this one-dimensional periodic rod, and $[0,\ \pi/l]$ denotes the irreducible Brillouin zone. The jth unit cell, consisting of a lumped mass and an attached local resonator, is selected for dynamic analysis.

The equations of motion of the lumped mass and the resonator can be written as

$$(M + m_r)\frac{\mathrm{d}^2u_j}{\mathrm{d}t^2} + 2ku_j - ku_{j-1} - ku_{j+1} + m_r\frac{\mathrm{d}^2x_j}{\mathrm{d}t^2} = 0 \tag{7}$$

$$m_r\frac{\mathrm{d}^2x_j}{\mathrm{d}t^2} + c\frac{\mathrm{d}x_j}{\mathrm{d}t} + f_{\mathrm{HSLDS}}(x_j) + m_r\frac{\mathrm{d}^2u_j}{\mathrm{d}t^2} = 0 \tag{8}$$

where M is the lumped mass of the$j$th unit cell, k is the equivalent stiffness of the connecting spring between the$j$th and $(j+1)$th lumped mass, m_r is the mass of the attached resonator, u_j is the displacement of the jth lumped mass, x_j is the displacement of the jth resonator mass relative to u_j, c and $f_{\mathrm{HSLDS}}(x_j)$ are the damping coefficient and restoring force of the resonator, respectively.

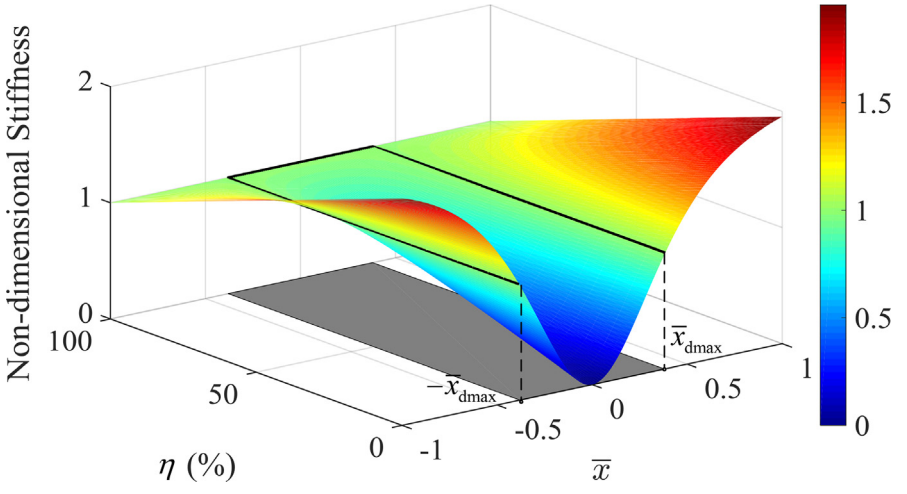

Fig. 3. Non-dimensional stiffness of the HSLDS resonator with different residual stiffness ratios η when $\bar{a} = (2/3)^{3/2}$. The gray area sketches the optimized low stiffness region.

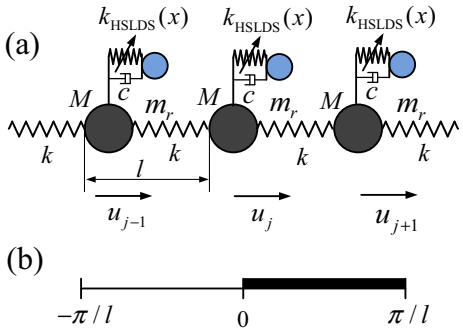

Fig. 4. (a) The lumped mass-spring model for the infinite-length HSLDS-LR periodic rod, and (b) the first Brillouin zone $[-\pi/l, \pi/l]$ and the irreducible Brillouin zone $[0, \pi/l]$ of the periodic rod.

By using the notations $\tau = \omega_0 t$, where $\omega_0 = \sqrt{k/M}$, $\alpha = m_r/M$ and $\beta = k_x/k$, Eqs. (7) and (8) can be rewritten as non-dimensional forms below

$$u_j'' + \frac{1}{1+\alpha}(2u_j - u_{j-1} - u_{j+1}) + \frac{\alpha}{1+\alpha}x_j'' = 0 \tag{9}$$

$$x_j'' + \frac{2\zeta}{\alpha}x_j' + v\bar{f}_{\mathrm{HSLDS}}\left(\bar{x}_j\right) + u_j'' = 0 \tag{10}$$

where $\zeta = c/\left(2\sqrt{Mk}\right)$ is the damping ratio, $v = \beta/\alpha$, the prime $(\cdot)'$ denotes differentiation with respect to τ, and $\bar{f}_{\mathrm{HSLDS}}\left(\bar{x}_j\right)$ represents the non-dimensional restoring force of the HSLDS resonator, which can be written as

$$\bar{f}_{\mathrm{HSLDS}}\left(\bar{x}\right) = \left[1 - (1-\eta)\frac{\bar{a}}{1-\bar{a}}\left(\frac{1}{\sqrt{\bar{a}^2 + \bar{x}^2}} - 1\right)\right]\bar{x} \tag{11}$$

In order to facilitate the subsequent dynamic analyses and calculations, the expression of the restoring force is simplified as a polynomial form

$$\bar{f}^{a}_{\mathrm{HSLDS}}(x_j) = \eta\bar{x}_j + \frac{(1-\eta)\bar{x}_j^3}{2\bar{a}^2\left(1-\bar{a}\right)} \tag{12}$$

Introducing a parameter $p = (1-\eta)/\left[2\bar{a}^2\left(1-\bar{a}\right)\right]$ to characterize the degree of the nonlinearity, Eq. (12) can be rewritten as

$$\bar{f}^{a}_{\mathrm{HSLDS}}(x_j) = \eta\bar{x}_j + p\bar{x}_j^3 \tag{13}$$

The comparison between the exact and approximate expressions of the restoring force is illustrated in Fig. 5. It can be found that the closer to 1 the value of η is, the smaller the difference becomes. Especially, the difference is 0 when $\eta = 1$, because the system degrades as a linear system in such a situation. Additionally, the difference increases steeply when

Table 1
Parameters of the HSLDS-LR periodic rod.

Parameters	Descriptions	Magnitude	Unit
E_1	Modulus of elasticity of the rubber	7.8	MP_a
E_2	Modulus of elasticity of the frame	69	GP_a
ρ_1	Density of the rubber	1.23×10^3	kg/m^3
ρ_2	Density of the frame	2.7012×10^3	kg/m^3
A	Effective area	5×10^{-3}	m^2
l	Lattice constant	0.158	m
k	Equivalent stiffness	6.67×10^4	N/m
M	Equivalent mass	0.089	kg
m_r	Mass of the resonator	0.0267	Kg
b_0	Length of oblique spring	36.74×10^{-3}	m

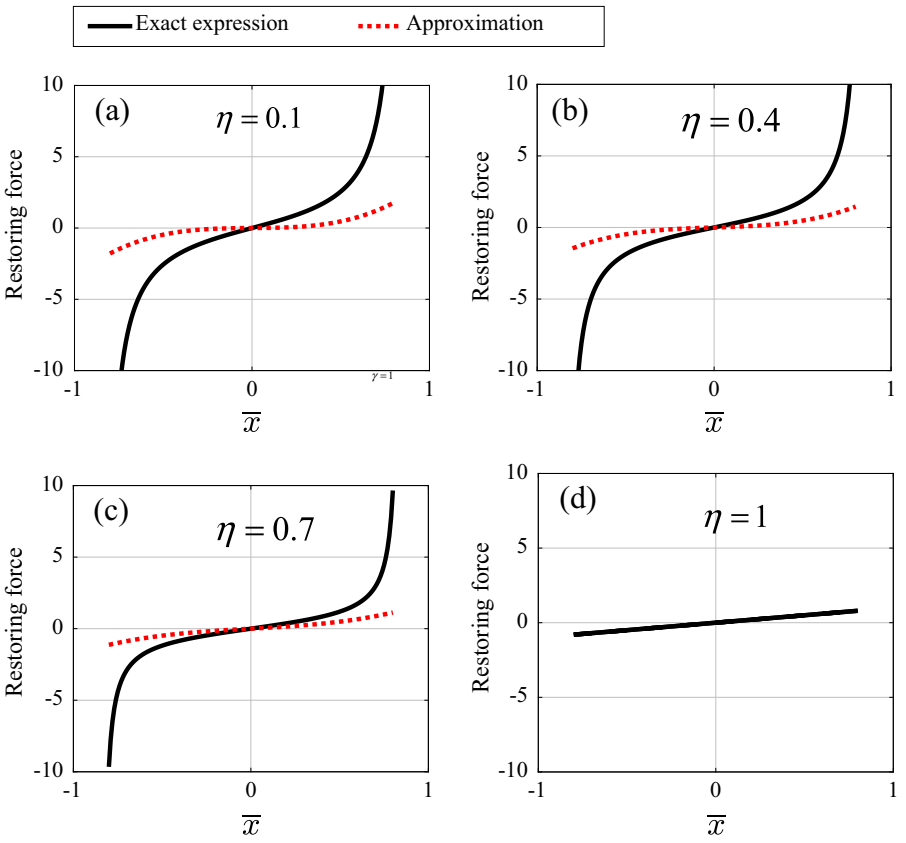

Fig. 5. Approximate expression of the restoring force $\bar{f}^{a}_{\mathrm{HSLDS}}$ of the HSLDS resonator compared with the exact one $\bar{f}_{\mathrm{HSLDS}}$ when (a) $\eta = 0.1$, (b) $\eta = 0.4$, (c) $\eta = 0.7$, (d) $\eta = 1$.

the mass of the resonator moves far away from the equilibrium position; however, for a small deviation, the approximation of the restoring force matches well with the exact one. Therefore, the approximate expression, i.e. Eq. (13), will be utilized for nonlinear dynamic analysis in Section 3.3.

3.2. The undamped linearized case

According to the static analysis of the HSLDS resonator (Fig. 3), the non-dimensional stiffness of the HSLDS resonators is close to a constant η in the vicinity of the equilibrium position. Therefore, the linearized stiffness of the HSLDS resonator is used to analyze band structures of the HSLDS-LR periodic rod under small-amplitude oscillations. In addition, the damping of the HSLDS resonator is not considered here. Therefore, for the undamped linearized system, the equation of motion of the jth resonator can be written as

$$x_j'' + \eta v x_j + u_j'' = 0 \tag{14}$$

By analogy with the monatomic chain, the displacement of the$j$th lumped mass can be written in the form of a traveling wave solution [37]

$$u_j = \mathrm{Z}e^{\mathrm{i}(jql-\Omega\tau)} \tag{15}$$

where Z is the oscillation amplitude, $\Omega = \omega/\omega_0$ is the frequency ratio of the excitation frequency ω to the natural frequency $\omega_0 = \sqrt{k/M}$ of the unit cell of the lumped mass-spring model, l is the lattice constant and q is the wave number of the longitudinal wave. According to the theorem of lattice vibration [37], two adjacent atoms vibrate with the same amplitude but with a phase difference. Therefore, the displacements of the $(j-1)$th and $(j+1)$th lumped masses can be given by

$$u_{j-1} = \mathrm{Z}e^{\mathrm{i}[(j-1)ql-\Omega\tau]}, \quad u_{j+1} = \mathrm{Z}e^{\mathrm{i}[(j+1)ql-\Omega\tau]} \tag{16}$$

Substituting Eqs. (16) and (15) into Eqs. (9) and (14), the displacement of the mass of the$j$th resonator can be written as

$$x_j = \frac{1}{\alpha\eta\nu} Z_j e^{i(jql-\Omega\tau)} \left(-\Omega^2 + 2 - e^{ql} - e^{-ql}\right) \tag{17}$$

Substituting Eqs. (15) and (17) into Eq. (14) and using the identity $\cosh(ql) = (e^{ql} + e^{-ql})/2$, the dispersion relation of the HSLDS-LR periodic rod can be given by

$$\cosh(ql) = 1 + \frac{\Omega^4 - (\nu+\beta)\eta\Omega^2}{2\left(\nu\eta - \Omega^2\right)} \tag{18}$$

Note that, the above dispersion relation is independent of the mass index j and displacement amplitude Z, but it can be influenced by stiffness ratio β and mass ratio α. Therefore, one can tune the band gaps by adjusting the stiffness ratio and mass ratio. For a given frequency, the wave propagation constant ql can be obtained by solving Eq. (18), as shown in Fig. 6, which illustrates the dispersion feature and band structure of the HSLDS-LR periodic rod. The solution of the propagation constant ql is complex. Assuming that the solution is written as $ql = Q_1 + iQ_2$ and substituting it into the displacement of the jth lumped mass, one can obtain $u_j = Ze^{i[j(Q_1+iQ_2)-\Omega\tau]} = Ze^{-jQ_2}e^{i(jQ_1-\Omega\tau)}$. Obviously, the real component Q_1

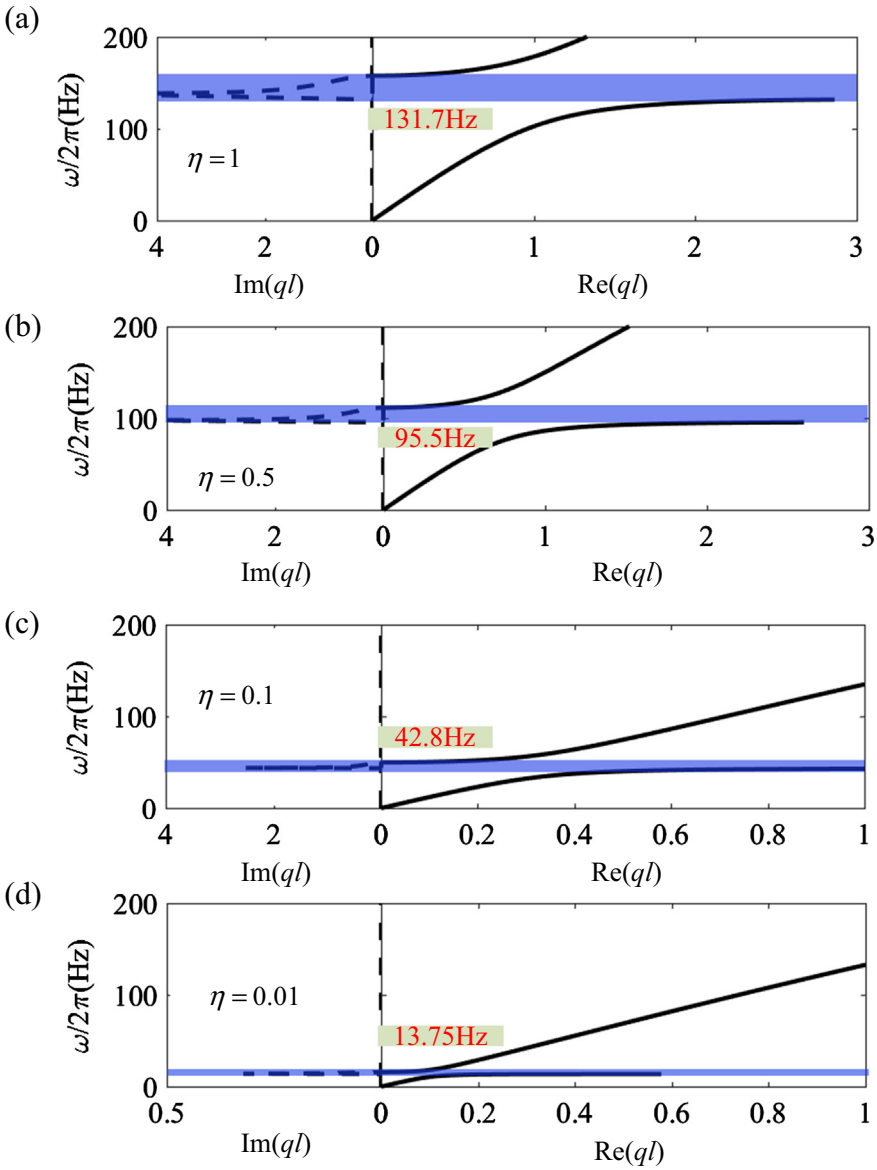

Fig. 6. Theoretical band gaps of the undamped linearized case for different residual stiffness when the mass ratio $\alpha = 0.3$ and the stiffness ratio $\beta = 0.3$. (a) $\eta = 1$, (b) $\eta = 0.5$, (c) $\eta = 0.1$, (d) $\eta = 0.01$.

decides the propagation direction, called phase constant, while the imaginary component Q_2 decides the wave attenuation, called attenuation constant. Additionally, with the decrease in the imaginary component of ql (Q_2), the wave attenuation becomes less effective. The band gaps are highlighted by shaded areas in Fig. 6.

Obviously, both the position and width of the band gaps are dependent on the residual stiffness of the HSLDS resonator, due to the fact that, for a local resonance band gap, its edging frequencies are determined by the resonant frequency, as given by [38]

$$\begin{aligned}\omega_{beginning} &= \sqrt{\frac{\eta k_x}{m_r}} \\ \omega_{ending} &= \sqrt{\frac{\eta k_x (M+m_r)}{M m_r}}\end{aligned} \tag{19}$$

where $\omega_{beginning}$ denotes the beginning frequency, namely the lower edge, and ω_{ending} the ending frequency, namely the upper edge of the band gap. Note that the normalized band, defined as $(\omega_{ending} - \omega_{beginning})/\omega_{beginning}$, is independent of the net stiffness ratio. Therefore, with the decrease in the net stiffness ratio, the normalized band keeps unchanged.

According to Eq. (19), one can find that when the residual stiffness of the HSLDS resonator decreases from 1 to 0, the position of the band gap moves towards a lower frequency and the bandwidth becomes narrower. For example, the beginning frequency of the band gap is 131.7 Hz when $\eta = 1$, and it moves towards 13.75 Hz when the dimensionless stiffness is tuned to $\eta = 0.01$, i.e. a hundredth of the stiffness of the horizontal spring that provides the positive stiffness. For the periodic chain without any attached resonators, constructed by removing all resonator from the HSLDS-LR chain, the center frequency of the BS band gap is $2\omega_0$ [3], i.e. 275.56 Hz. Therefore, the HSLDS resonator is capable of shifting the band gap towards a very low frequency by tuning its net stiffness.

3.3. The damped nonlinear case

In this section, the nonlinearity of the stiffness [28] and the damping [39] are taken into account, and its effect on the wave propagation properties will be studied in detail. The Harmonic Balance method is used to solve the nonlinear equations of motion of the nonlinear HSLDS-LR rod, and then the feature of nonlinear wave propagation alone this periodic rod is revealed.

Considering the fundamental harmonic response only, the displacement of the mass of the jth HSLDS resonator in the form of complex Fourier series can be given as

$$x_j(\tau) = A_{k,j} e^{i\Omega\tau} + \bar{A}_{k,j} e^{-i\Omega\tau} \tag{20}$$

Substituting Eq. (20) into Eqs. (9) and (10) and integrating twice with respect toτ, one can obtain the displacement of the$j$th lumped mass, as given by

$$u_j(t) = \left(-A_{1,j} + \frac{\eta v A_{1,j}}{\Omega^2} + \frac{2i\zeta A_{1,j}}{\beta\Omega} + \frac{3pvA_{1,j}^2 \bar{A}_{1,j}}{\Omega^2} \right) e^{i\Omega\tau} \tag{21}$$

According to the Bloch theorem [40], the displacements of the $(j-1)$th lumped mass and $(j+1)$th lumped mass can be given by

$$u_{j-1} = \left(-A_{1,j} + \frac{\eta v A_{1,j}}{\Omega^2} + \frac{2i\zeta A_{1,j}}{\beta\Omega} + \frac{3pvA_{1,j}^2 \bar{A}_{1,j}}{\Omega^2} \right) e^{-ql} e^{i\Omega\tau} \tag{22}$$

$$u_{j+1} = \left(-A_{1,j} + \frac{\eta v A_{1,j}}{\Omega^2} + \frac{2i\zeta A_{1,j}}{\beta\Omega} + \frac{3pvA_{1,j}^2 \bar{A}_{1,j}}{\Omega^2} \right) e^{ql} e^{i\Omega\tau} \tag{23}$$

Substituting Eqs. (20–23) into Eqs. (9) and (10), and using the identity $\cosh(ql) = (e^{ql} + e^{-ql})/2$ again, a nonlinear dispersion relation for the HSLDS-LR periodic rod can be given by

$$\cosh(ql) = 1 - \frac{(1+\alpha)\Omega^2}{2} - \frac{1}{2} \frac{\alpha^2\Omega^4}{-\alpha\Omega^2 + \beta\eta + 2i\zeta\Omega + 3\beta p A_{1,j} \bar{A}_{1,j}} \tag{24}$$

Compared with the undamped linearized case, the damping and the nonlinearity are included in the dispersion relation for the nonlinear case. The effect of damping on the dispersion relation for different nonlinear parameters is illustrated in Fig. 7. The black and pink arrows represent the center frequencies of the band gap for the damped linearized case and damped nonlinear case, respectively. Obviously, as the damping ratio increases, the magnitude of the imaginary component of ql in the band gap reduces for both the damped linearized case (Fig. 7a) and damped nonlinear case (Fig. 7b–d), which

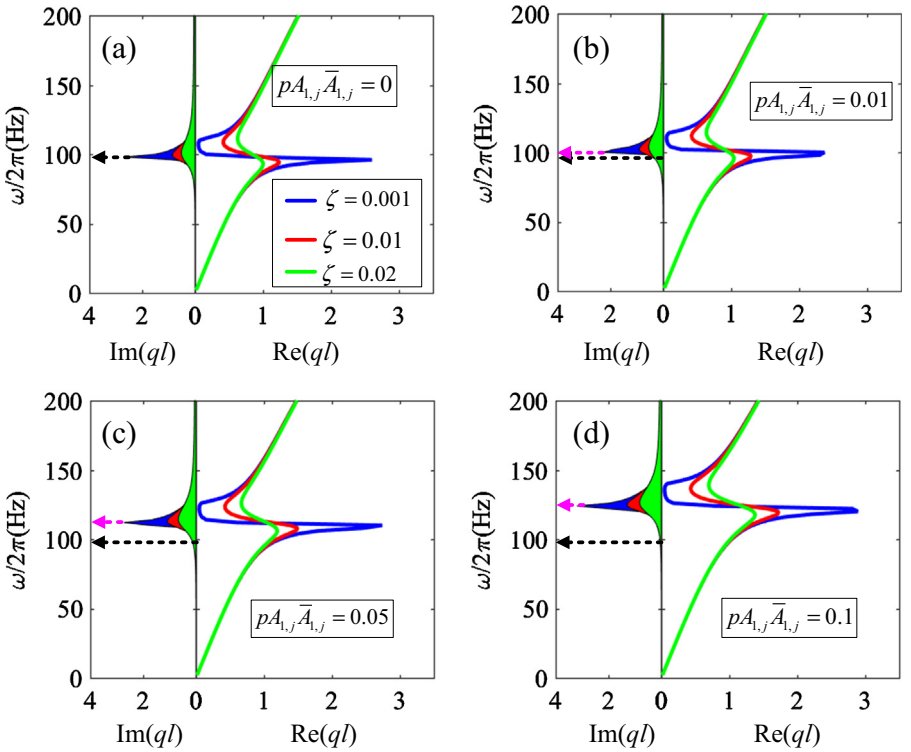

Fig. 7. Dispersion relation of the one-dimensional chain influenced by damping ratios for different nonlinear parameters (a) $pA_{1,j}\bar{A}_{1,j}=0$, (b) $pA_{1,j}\bar{A}_{1,j}=0.01$, (c) $pA_{1,j}\bar{A}_{1,j}=0.05$ and (d) $pA_{1,j}\bar{A}_{1,j}=0.1$ when the residual stiffness ratio $\eta=0.5$.

implies the wave attenuation becomes worse, but the bandwidth becomes wider. This is an inherent influence of damping on the performance of a local resonator. So that adding damping into the HSLDS resonator would be useful to broaden the band gap.

In addition, the effect of the nonlinearity of the HSLDS resonator on the band gap is represented in Fig. 8. As seen from Fig. 8, the impact of nonlinearity on the position of band gap is more significant than damping ratio. The blue line and area denote the dispersion relation when nonlinear parameter $pA_{1,j}\bar{A}_{1,j}$ is 0.01, the red 0.05 and green 0.1. Regardless of the amount of damping ratio, the location of the band gap moves towards higher frequencies and the bandwidth is broadened when the nonlinearity becomes stronger. This can be attributed to the hardening-stiffness feature of the HSLDS resonator. In other words, as the oscillation amplitude increases, the stiffness becomes larger.

Fig. 9 shows the dispersion relations in the undamped linearized case (Fig. 9a), undamped nonlinear case (Fig. 9b), damped linearized case (Fig. 9c) and damped nonlinear case (Fig. 9d). It can be seen that the band gap is widened and the wave attenuation is enhanced by increasing the mass ratio, when the resonant frequency is kept unchanged by increasing the stiffness by the same proportion. In fact, this observation is an intrinsic characteristic of local resonance, namely, both the ending frequency of the band gap and the wave attenuation at the resonant frequency are positively correlated to the mass ratio [41,42].

3.4. Numerical verification

In order to validate the theoretical analysis, numerical simulations are carried out by two ways. On the one hand, the equations of motion of the simplified lumped mass-spring chain (Eqs. (9) and (10)), are solved by using Matlab® function *ode45*; on the other hand, this chain is modeled and analyzed by using Adams®. Note that, for the lumped mass-spring chain, the response of the chain can be more easily and quickly obtained by using the multi-body dynamic simulation than by utilizing the finite element analysis.

Applying a displacement excitation on the left end of the lumped mass-spring chain (Fig. 4), the equations of motion can be rewritten as

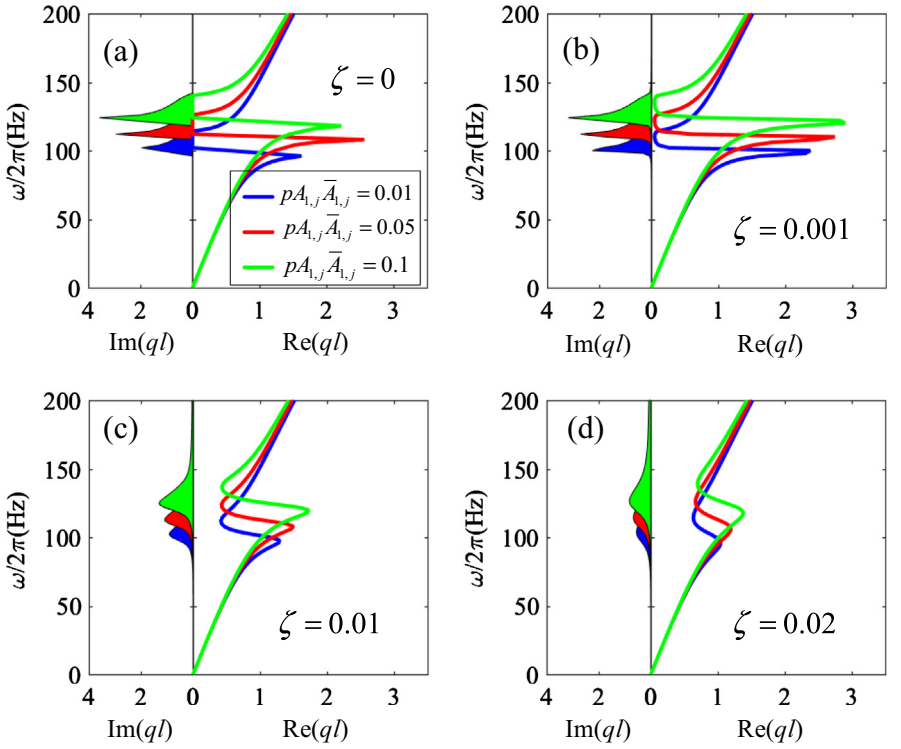

Fig. 8. Dispersion relation of the one-dimensional chain effected by nonlinear parameter for damping ratios (a) $\xi = 0$, (b) $\xi = 0.001$, (c) $\xi = 0.01$ and (d) $\xi = 0.02$ when the residual stiffness ratio $\eta = 0.5$.

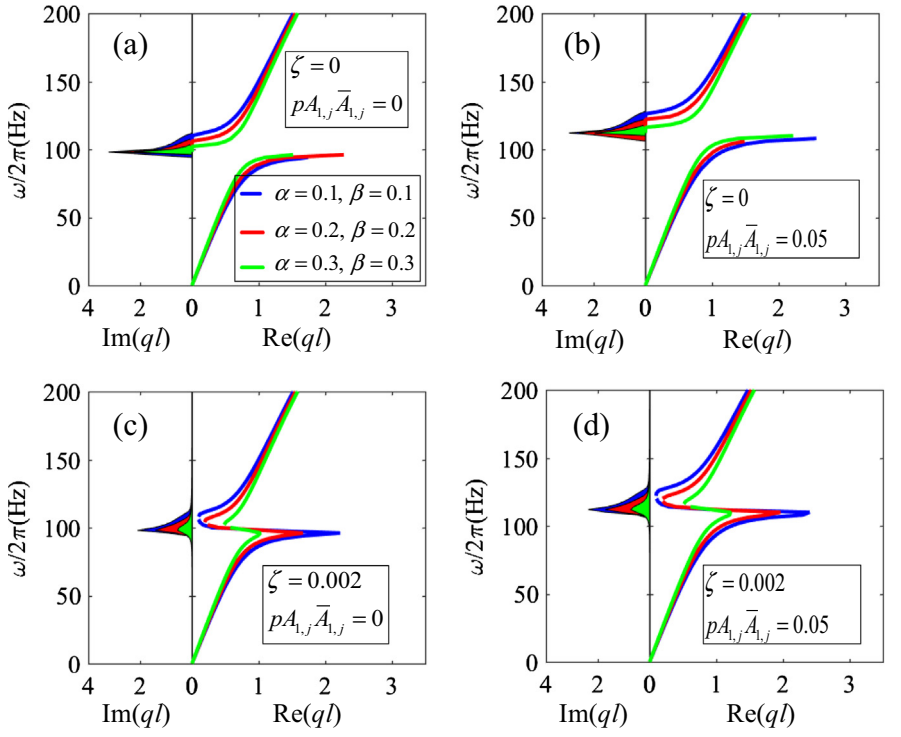

Fig. 9. Dispersion relation of the one-dimensional chain influenced by mass ratio and stiffness ratio for (a) undamped linearized case, (b) undamped nonlinear case, (d) damped linearized case and (c) damped nonlinear case when the residual stiffness ratio $\eta = 0.5$.

$$\begin{cases} u_j'' + \frac{1}{1+\beta}(u_j - u_{j+1}) + \frac{\beta}{1+\beta}x_j'' = 0 & j = 1, \\ u_j'' + \frac{1}{1+\beta}(2u_j - u_{j-1} - u_{j+1}) + \frac{\beta}{1+\beta}x_j'' = 0, & 2 \le j \le n-1, \\ u_j'' + \frac{1}{1+\beta}(u_j - u_{j-1}) + \frac{\beta}{1+\beta}x_j'' = 0, & j = n. \end{cases} \tag{25}$$

$$x_j'' + \frac{2\zeta}{\beta}x_j' + \bar{vf}_{\mathrm{HSLDS}}(x_j) + u_j'' = 0 \tag{26}$$

Note that the actual nonlinear stiffness of the HSLDS resonator, i.e. Eq. (11), is used rather than the approximate one, and damping is also taken into account to dampen transient responses.

The boundary condition of this chain is free-free. In order to avoid rigid-body motion, the first unit cell is excited by a time-harmonic displacement rather than a force. Therefore, the displacement and velocity boundary conditions of the first unit cell can be given by [43]

$$u_1 = \bar{Z}_1 \cos(\Omega\tau), \quad u_1' = -\bar{Z}_1 \Omega \sin(\Omega\tau) \tag{27}$$

where $\bar{Z}_1 = Z_1/b_0$ is the displacement amplitude in dimensionless form. Solving Eqs. (25) and (26) by the Runge-Kutta method embedded in *ode45*, the responses of each lumped mass and resonators can be obtained. In the numerical simulations, the number of unit cells is selected to be eight. The wave attenuation performance is evaluated by wave transmittance in decibel (dB), which is defined as the ratio of the root-mean-squared (RMS) displacement of the right-end (eighth) lumped mass to that of the left-end (first) lumped mass.

The numerical simulations are reported in Fig. 10, where the solid lines denote multi-body dynamic simulations by using Adams®, and the dotted lines represent numerical results by solving the equations of motion. From Fig. 10, one can observe good agreement between the results obtained by these two methods. Nevertheless, the difference would increase when the non-dimensional stiffness of the resonator is tuned from 1 to 0, which can be attributed to the fact that the nonlinearity of the resonator becomes significant when its stiffness is reduced, as illustrated in Fig. 3, but the nonlinearity cannot be taken into account when the multi-body dynamic simulations are carried out by Adams®.

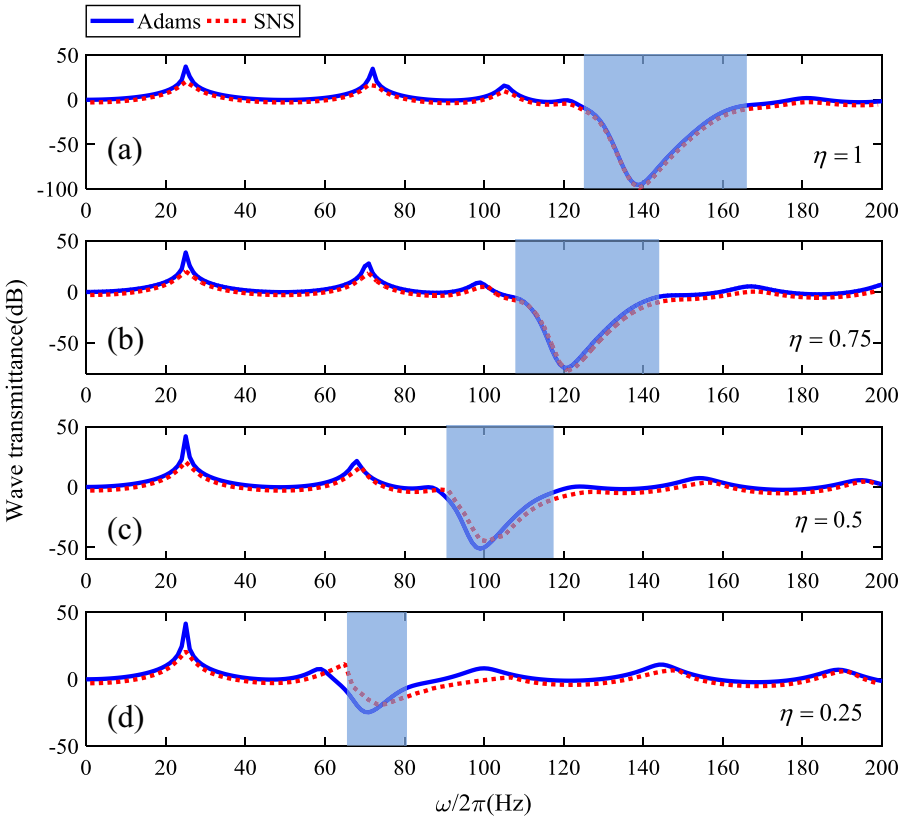

Fig. 10. Comparison of wave transmittance between numerical simulations (SNS) and multi-body dynamic simulations (Adams®) for (a) $\eta = 1$, (b) $\eta = 0.75$, (c) $\eta = 0.5$, (d) $\eta = 0.25$ when the number of the unit cell $n = 8$ and the damping ratio $\zeta = 0.01$. Shadow areas denote the band gaps.

Furthermore, the wave transmittance in dB is less than zero when the excitation frequency locates in the band gap marked by the shade area, which implies wave attenuation, namely, the displacement amplitude at the end of the lumped mass-spring chain is smaller than the excitation amplitude. Note that, the band gap in this figure is determined by finding an area in which the wave transmittances are less than zero and equal to zero at the lower and upper edges. As shown Fig. 11, the blue lines with pentagrams and triangles denote the ending frequency (EF) and beginning frequency (BF) of the band gap obtained by the analytical analyses in Section 3.2, respectively. And the red lines with squares and hexagons indicate the EF and BF by numerical simulations, respectively. The difference between the BF and EF demonstrates the band gap. From this figure, it can be found that the band gap revealed by the numerical simulations matches well with the theoretical ones, although the linearized stiffness is used in the analytical analyses. Therefore, the analytical dispersion relations of the linearized system can be utilized to demonstrate the band structure of the HSLDS-LR periodic rod. Most importantly, as mentioned in Section 3.2, the band gap induced by the proposed HSLDS local resonator can be created at a very low frequency region by employing the NS mechanism to reduce its stiffness.

4. Wave attenuations by HSLDS local resonators

In order to find out the wave attenuation performance of the proposed resonator, this section will discuss influences of the number of unit cells and excitation amplitude on the longitudinal wave attenuation in the HSLDS-LR periodic rod.

4.1. Influence of the number of unit cells

The effect of the number of unit cells on wave attenuation is shown in Fig. 12, when $\eta = 0.5$, $\zeta = 0.001$ and $Z_1 = 1$ mm. In this figure, the wave attenuation is represented by the minus transmittance (in dB) on the contour map, which is calculated by using numerical simulations, and thus the band gap is shown by a belt with distinct colors in the vicinity of 100 Hz. Obviously, as the number of unit cells increases, the band gap becomes wider, and the wave attenuation performance is enhanced notably. Also shown is that more resonant peaks occur as the number of unit cells increases, due to new emerging resonant frequencies of the system after adding more unit cells.

4.2. Influence of the excitation amplitude

As mentioned in Section 2, the stiffness of the HSLDS resonator is nonlinear and related to the displacement. When the resonator undergoes large-amplitude vibration, both the location and width of the band gap would change with the variation of the excitation amplitude. Fig. 13 shows the effect of the excitation amplitude on the wave transmittance, which is also obtained by numerical simulations. From Fig. 13a, a wide and deep band gap can be observed under a small-amplitude excitation. When the excitation amplitude increases, the band gap moves to high frequencies, as shown in Fig. 13b–d, which agrees well with the theoretical observation in Fig. 8.

However, the width and depth of the band gap are reduced by increasing excitation amplitude, leading to worse wave attenuation performance, which is opposite to theoretical results in Fig. 8. The reason for this disparity is that only the fundamental harmonic is considered in the theoretical analyses, but in the numerical simulations, sub-harmonics, superharmonics, or even chaos would appear, when the nonlinear system is under large excitations. Therefore, in order to achieve a targeted band gap, large-amplitude oscillations of the HSLDS resonator should be avoided as much as possible.

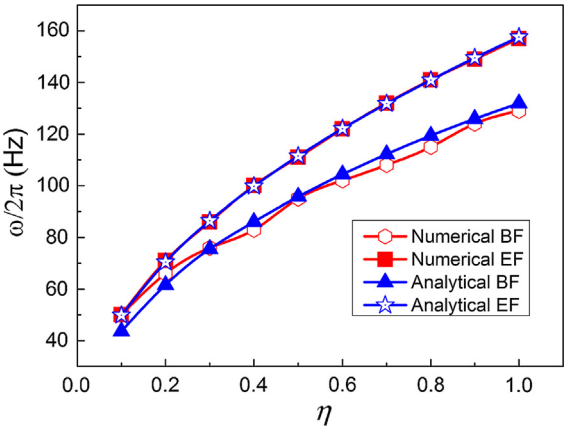

Fig. 11. Band structures for different residual stiffness ratios η calculated both analytically and numerically, when the number of unit cells $n = 8$, the mass ratio $\alpha = 0.3$, the stiffness ratio $\beta = 0.3$ and the damping ratio $\zeta = 0.001$. The analytical ending frequency (EF) and beginning frequency (BF) are denoted by stars and triangles, respectively, while the numerical EF and BF by squares and hexagons, respectively.

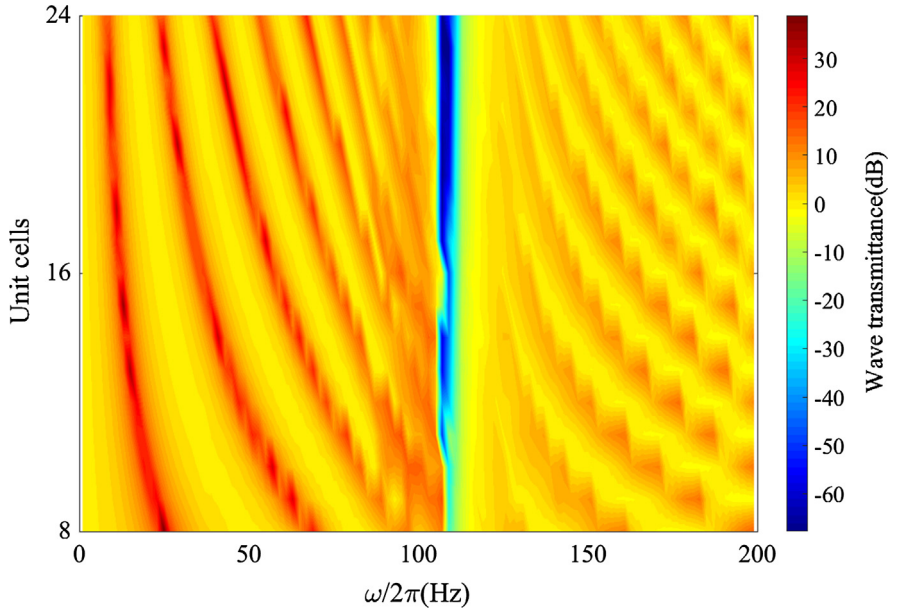

Fig. 12. Wave transmittance of the HSLDS-LR rod for different numbers of unit cells when the damping ratio $\zeta = 0.001$, the displacement amplitude $Z_1 = 1$ mm and the residual stiffness ratio $\eta = 0.5$.

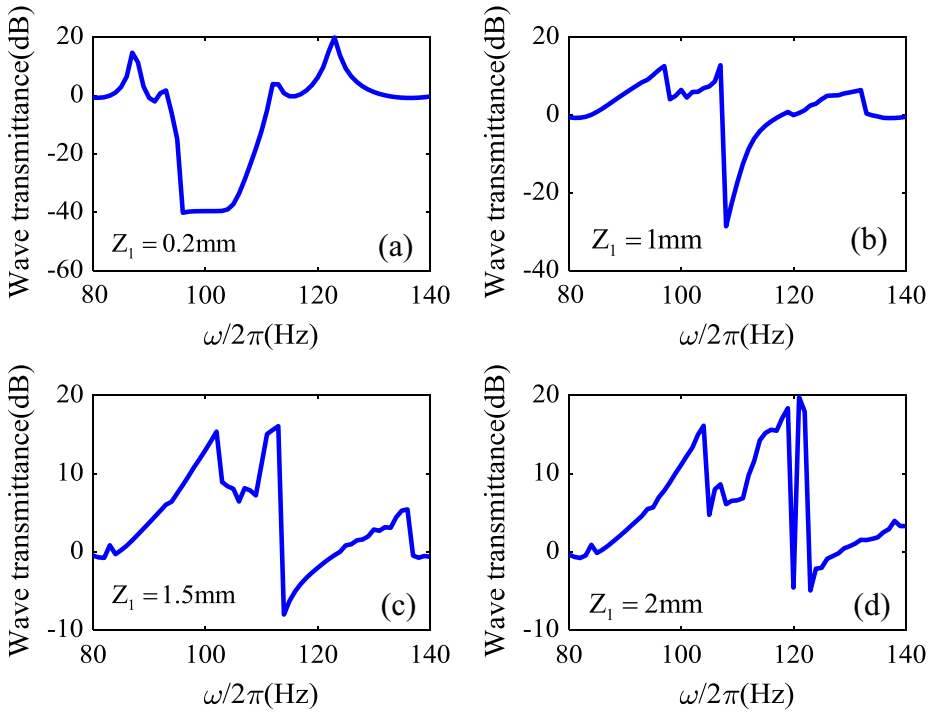

Fig. 13. Influences of excitation amplitude on the wave transmittance of the HSLDS-LR rod with 8 unit cells and the damping ratio $\zeta = 0.001$, the residual stiffness ratio $\eta = 0.5$.

5. Conclusions

In this paper, a high-static-low-dynamic-stiffness (HSLDS) local resonator with geometrical nonlinearity is proposed to lower the band gap of longitudinal waves propagating in a one-dimensional periodic rod. The HSLDS-LR periodic rod is

modeled as a lumped mass-spring chain to analyze its dispersion relation and reveal the band structure, which is validated by numerical simulations and multi-body dynamic simulations. Several conclusions are drawn as follows.

Firstly and most importantly, the stiffness of proposed HSLDS local resonator can be tuned towards an ultra-low targeted value by employing negative-stiffness mechanisms, and thus the longitudinal wave band gap can be significantly shafted from high into very low-frequency range. This conceptual design can be considered as a potential solution for very low-frequency wave and vibration manipulation, such as longitudinal wave filter and mechanical vibration isolator. Furthermore, the width and depth of the band gap are related to the mass ratio, nonlinearity and damping ratio of the HSLDS resonator, and a large mass ratio and a small damping ratio are favorable. In addition, a sufficient number of unit cells are needed to form wide and deep band gaps. A large excitation might induce complicated responses, leading to worse wave attenuating capability; therefore, large-amplitude oscillations of the HSLDS resonator should be avoided as much as possible.

Acknowledgments

This research work was supported by National Key R&D Program of China (2017YFB1102801), National Natural Science Foundation of China (11572116), Natural Science Foundation of Hunan Province (2016JJ3036) and Hunan Provincial Innovation Foundation for Postgraduate. The first author, Kai Wang, would like to thank the support from the China Scholarship Council (CSC).

References

[1] M.M. Sigalas, E.N. Economou, Elastic and acoustic wave band structure, J. Sound Vib. 158 (1992) 377–382, https://doi.org/10.1016/0022-460X(92)90059-7.
[2] Z. Liu, X. Zhang, Y. Mao, Y.Y. Zhu, Z. Yang, C.T. Chan, P. Sheng, Locally resonant sonic materials, Science (80-) 289 (2000) 1734–1736, https://doi.org/10.1126/science.289.5485.1734.
[3] M.I. Hussein, M.J. Leamy, M. Ruzzene, Dynamics of phononic materials and structures: historical origins, recent progress, and future outlook, Appl. Mech. Rev. 66 (2014) 040802, https://doi.org/10.1115/1.4026911.
[4] D. Yu, J. Wen, H. Zhao, Y. Liu, X. Wen, Vibration reduction by using the idea of phononic crystals in a pipe-conveying fluid, J. Sound Vib. 318 (2008) 193–205, https://doi.org/10.1016/j.jsv.2008.04.009.
[5] E.D. Nobrega, F. Gautier, A. Pelat, J.M.C. Dos Santos, Vibration band gaps for elastic metamaterial rods using wave finite element method, Mech. Syst. Signal Process. 79 (2016) 192–202, https://doi.org/10.1016/j.ymssp.2016.02.059.
[6] S. Zuo, T. Ni, X. Wu, J. Fan, Studies of band gaps in flexural vibrations of a locally resonant beam with novel multi-oscillator configuration, J. Vib. Control. 23 (2015) 1663–1674, https://doi.org/10.1177/1077546315598032.
[7] M.Y. Wang, X. Wang, Frequency band structure of locally resonant periodic flexural beams suspended with force–moment resonators, J. Phys. D. Appl. Phys. 46 (2013) 255502, https://doi.org/10.1088/0022-3727/46/25/255502.
[8] X. Wang, M.Y. Wang, An analysis of flexural wave band gaps of locally resonant beams with continuum beam resonators, Meccanica 51 (2016) 171–178, https://doi.org/10.1007/s11012-015-0197-x.
[9] Y. Xiao, J. Wen, L. Huang, X. Wen, Analysis and experimental realization of locally resonant phononic plates carrying a periodic array of beam-like resonators, J. Phys. D Appl. Phys. 47 (2014) 045307, https://doi.org/10.1088/0022-3727/47/4/045307.
[10] N.M.M. Frandsen, O.R. Bilal, J.S. Jensen, M.I. Hussein, Inertial amplification of continuous structures: Large band gaps from small masses, J. Appl. Phys. 119 (2016) 124902, https://doi.org/10.1063/1.4944429.
[11] G. Wang, S. Chen, J. Wen, Low-frequency locally resonant band gaps induced by arrays of resonant shunts with Antoniou's circuit: experimental investigation on beams, Smart Mater. Struct. 20 (2011) 015026, https://doi.org/10.1088/0964-1726/20/1/015026.
[12] B. Bao, D. Guyomar, M. Lallart, Vibration reduction for smart periodic structures via periodic piezoelectric arrays with nonlinear interleaved-switched electronic networks, Mech. Syst. Signal Process. 82 (2017) 230–259, https://doi.org/10.1016/j.ymssp.2016.05.021.
[13] X. Zhou, C. Chen, Tuning the locally resonant phononic band structures of two-dimensional periodic electroactive composites, Phys. B Condens. Matter. 431 (2013) 23–31, https://doi.org/10.1016/j.physb.2013.08.042.
[14] E. Coffy, T. Lavergne, M. Addouche, S. Euphrasie, P. Vairac, A. Khelif, Ultra-wide acoustic band gaps in pillar-based phononic crystal strips, J. Appl. Phys. 118 (2015) 214902, https://doi.org/10.1063/1.4936836.
[15] T. Wang, M.P. Sheng, Q.H. Qin, Multi-flexural band gaps in an Euler-Bernoulli beam with lateral local resonators, Phys. Lett. A 380 (2016) 525–529, https://doi.org/10.1016/j.physleta.2015.12.010.
[16] P.F. Pai, H. Peng, S. Jiang, Acoustic metamaterial beams based on multi-frequency vibration absorbers, Int. J. Mech. Sci. 79 (2014) 195–205, https://doi.org/10.1016/j.ijmecsci.2013.12.013.
[17] M.Y. Wang, Y.T. Choy, C.W. Wan, A.S. Zhao, Wide band-gaps in flexural periodic beams with separated force and moment resonators, J. Vib. Acoust. 137 (2015) 064504, https://doi.org/10.1115/1.4031519.
[18] J.X. Zhou, K. Wang, D.L. Xu, H.J. Ouyang, Y.L. Li, A six degrees-of-freedom vibration isolation platform supported by a hexapod of quasi-zero-stiffness struts, J. Vib. Acoust. 139 (2017) 34502, https://doi.org/10.1115/1.4035715.
[19] X. Sun, X. Jing, Multi-direction vibration isolation with quasi-zero stiffness by employing geometrical nonlinearity, Mech. Syst. Signal Process. 62–63 (2015) 149–163, https://doi.org/10.1016/j.ymssp.2015.01.026.
[20] K. Wang, J. Zhou, D. Xu, Sensitivity analysis of parametric errors on the performance of a torsion quasi-zero-stiffness vibration isolator, Int. J. Mech. Sci. 134 (2017) 336–346, https://doi.org/10.1016/j.ijmecsci.2017.10.026.
[21] Y.C. Wang, R.S. Lakes, Extreme stiffness systems due to negative stiffness elements, Am. J. Phys. 72 (2004) 40–50, https://doi.org/10.1119/1.1619140.
[22] Z. Hao, Q. Cao, M. Wiercigroch, Nonlinear dynamics of the quasi-zero-stiffness SD oscillator based upon the local and global bifurcation analyses, Nonlinear Dyn. 87 (2016) 987–1014, https://doi.org/10.1007/s11071-016-3093-6.
[23] Z. Hao, Q. Cao, M. Wiercigroch, Two-sided damping constraint control strategy for high-performance vibration isolation and end-stop impact protection, Nonlinear Dyn. 86 (2016) 2129–2144, https://doi.org/10.1007/s11071-016-2685-5.
[24] Q.J. Cao, M. Wiercigroch, E.E. Pavlovskaia, C. Grebogi, J.M.T. Thompson, Archetypal oscillator for smooth and discontinuous dynamics, Phys. Rev. E 74 (2006) 046218, https://doi.org/10.1103/PhysRevE.74.046218.
[25] Z. Hao, Q.J. Cao, A novel dynamical model for gvt nonlinear supporting system with stable-quasi-zero-stiffness, J. Theor. Appl. Mech. (2014) 199–213.
[26] J. Zhou, K. Wang, D. Xu, H. Ouyang, Multi-low-frequency flexural wave attenuation in Euler-Bernoulli beams using local resonators containing negative-stiffness mechanisms, Phys. Lett. Sect. A Gen. At. Solid State Phys. 381 (2017) 3141–3148, https://doi.org/10.1016/j.physleta.2017.08.020.
[27] J. Zhou, K. Wang, D. Xu, H. Ouyang, Local resonator with high-static-low-dynamic stiffness for lowering band gaps of flexural wave in beams, J. Appl. Phys. 121 (2017) 044902, https://doi.org/10.1063/1.4974299.

[28] B.S. Lazarov, J.S. Jensen, Low-frequency band gaps in chains with attached non-linear oscillators, Int. J. Non. Linear. Mech. 42 (2007) 1186–1193, https://doi.org/10.1016/j.ijnonlinmec.2007.09.007.
[29] X. Fang, J. Wen, J. Yin, D. Yu, Y. Xiao, Broadband and tunable one-dimensional strongly nonlinear acoustic metamaterials: theoretical study, Phys. Rev. E. 94 (2016) 1–10, https://doi.org/10.1103/PhysRevE.94.052206.
[30] G. Chakraborty, A.K. Mallik, Dynamics of a weakly non-linear periodic chain, Int. J. Non. Linear. Mech. 36 (2001) 375–389, https://doi.org/10.1016/S0020-7462(00)00024-X.
[31] K.L. Manktelow, M.J. Leamy, M. Ruzzene, Weakly nonlinear wave interactions in multi-degree of freedom periodic structures, Wave Motion 51 (2014) 886–904, https://doi.org/10.1016/j.wavemoti.2014.03.003.
[32] V.M. Rothos, A.F. Vakakis, Dynamic interactions of traveling waves propagating in a linear chain with an local essentially nonlinear attachment, Wave Motion 46 (2009) 174–188, https://doi.org/10.1016/j.wavemoti.2008.10.004.
[33] R. Khajehtourian, M.I. Hussein, Dispersion characteristics of a nonlinear elastic metamaterial, AIP Adv. 4 (2014) 124308, https://doi.org/10.1063/1.4905051.
[34] M.J. Frazier, D.M. Kochmann, Band gap transmission in periodic bistable mechanical systems, J. Sound Vib. 388 (2017) 315–326, https://doi.org/10.1016/j.jsv.2016.10.041.
[35] D. Kochmann, K. Bertoldi, Exploiting microstructural instabilities in solids and structures: from metamaterials to structural transitions, Appl. Mech. Rev. 69 (2017) 050801–50811, https://doi.org/10.1115/1.4037966.
[36] D. Cheng, Handbook of Mechanical Design [in Chinese], Chemical Industry Press, Beijing, 2015.
[37] L. Brillouin, Wave Propagation in Periodic Structures: Electric Filters and Crystal Lattices, Dover Publications Inc, New York, 2003.
[38] K. Wang, J. Zhou, X. Daolin, H. Ouyang, Tunable low-frequency torsional-wave band gaps in a meta-shaft, J. Phys. D Appl. Phys. 52 (2019) 055104, https://doi.org/10.1088/1361-6463/aaf039.
[39] M.I. Hussein, M.J. Frazier, Band structure of phononic crystals with general damping, J. Appl. Phys. 108 (2010) 093506, https://doi.org/10.1063/1.3498806.
[40] Y.Q. Guo, D.N. Fang, Analysis and interpretation of longitudinal waves in periodic multiphase rods using the method of reverberation-ray matrix combined with the Floquet-Bloch theorem, J. Vib. Acoust. 136 (2013) 011006, https://doi.org/10.1115/1.4025438.
[41] T.L. Smith, K. Rao, I. Dyer, Attenuation of plate flexural waves by a layer of dynamic absorbers, Noise Control Eng. J. 26 (1986) 56–60, https://doi.org/10.3397/1.2827662.
[42] D.J. Thompson, A continuous damped vibration absorber to reduce broad-band wave propagation in beams, J. Sound Vib. 311 (2008) 824–842, https://doi.org/10.1016/j.jsv.2007.09.038.
[43] N. Nadkarni, C. Daraio, D.M. Kochmann, Dynamics of periodic mechanical structures containing bistable elastic elements: from elastic to solitary wave propagation, Phys. Rev. E – Stat. Nonlinear, Soft Matter Phys. 90 (2014) 023204, https://doi.org/10.1103/PhysRevE.90.023204.